Nanoscale Structure of Self-Assembling Hybrid Materials of Inorganic and Electronically Active Organic Phases

Marina Sofos,[†] David A. Stone,[‡] Dipak K. Goswami,[†] John S. Okasinski,[†] Hua Jin,[†] Michael J. Bedzyk,[†] and Samuel I. Stupp*[,†,‡,§]

Department of Materials Science and Engineering, Department of Chemistry, and Feinberg School of Medicine, Northwestern University, Evanston, Illinois 60208

Received: September 20, 2007

Hybrid materials with nanoscale structure that incorporates inorganic and organic phases with electronic properties offer potential in an extensive functional space that includes photovoltaics, light emission, and sensing. This work describes the nanoscale structure of model hybrid materials with phases of silica and electronically active bola-amphiphile assemblies containing either oligo(*p*-phenylene vinylene) or oligo(thiophene) segments. The hybrid materials studied here were synthesized by evaporation-induced self-assembly and characterized by X-ray scattering techniques. Grazing-incidence X-ray scattering studies of these materials revealed the formation of two-dimensional hexagonally packed cylindrical micelles of the organic molecules with diameters between 3.1 and 3.6 nm and cylindrical axes parallel to the surface. During the self-assembly process at low pH, the cylindrical aggregates of conjugated molecules become surrounded by silica giving rise to a hybrid structure with long-range order. Specular X-ray reflectivity confirmed the long-range periodicity of the hybrid films within a specific range of molar ratios of tetraethyl orthosilicate to cationic amphiphile. We did not observe any long-range ordering in fully organic analogues unless quaternary ammonium groups were replaced by tertiary amines. These observations suggest that charge screening in these biscationic conjugated molecules by the mineral phase is a key factor in the evolution of long range order in the self-assembling hybrids.

Introduction

Nanocomposites of organic and inorganic components offer a strategy toward improved properties and novel functions of materials.[1,2] Historically, interest in hybrids has focused on tuning and optimization of mechanical properties, but more recently these materials have been of interest for other properties such as optical and electronic behavior,[3,4] light emission,[5−7] and photovoltaic function.[8−11] In these areas, the ordering of organic and inorganic domains and the nature of their interfaces on the nanoscale are especially critical to attain optimum function.

Among the various strategies used for synthesis of hybrids, molecular self-assembly is a powerful bottom-up method. In one self-assembly approach, the amphiphilicity of synthetic organic molecules is used to control nanoscale ordering of organic and inorganic domains.[12−15] For example, this can be accomplished by using the pre-ordered soft organic to guide the growth of inorganic components in hydrophilic domains and control their size, shape, and location. This particular strategy is inspired by biomineralization processes in nature,[16] and therefore, template-driven synthesis of hybrids is biomimetic in character.[17] Our own group has used amphiphilic lyotropic liquid crystalline templates to synthesize nanostructured II−VI semiconductors.[18,19] The resulting composite superlattice morphology directly copies the original organic matrix with the semiconductor forming in the hydrophilic regions and locking in the amphiphilic molecules. The amphiphilicity of organic molecules can also be used in a dynamic coassembly approach. In this case, the surfactants, at concentrations below their critical micelle concentrations, are mixed with inorganic precursors, and their interactions lead to organization at the nanoscale. Kresge et al. pioneered this strategy producing mesoporous silica after the organic component is removed from the pores.[20,21] With variations to the surfactant, inorganic precursors, and processing conditions, a number of mesoporous hybrids have been developed.[22,23] Such processing has since been extended to thin-film formation,[24−27] resulting in the one-step evaporation-induced self-assembly (EISA) process that relies on preferential solvent evaporation from dilute homogeneous solutions to form highly ordered mesophases.[28−30] The versatility of EISA can be further exploited by adding function to the organic surfactant, as has been shown, for example, with the use of polymerizable surfactants.[31−33] Nonionic conjugated surfactants,[34,35] as well as very low concentrations of charged conjugated surfactants,[36] have been incorporated into EISA systems in order to enhance fluorescence in hybrid materials.

Our group recently extended the utility of EISA by designing electronically active bola-amphiphiles that generate hybrid materials with remarkable energy-transfer properties.[37] In the original system we developed, the amphiphiles consist of an oligo(*p*-phenylene vinylene) (OPV) trimer moiety symmetrically substituted at the para position with a short alkyl tail terminated with a trimethylammonium bromide group. Similar bolaform OPV amphiphiles for the fabrication of light-emitting diodes,[38] as well as bolaform sexithiophene amphiphiles,[39−41] have been reported but were used in multistep layer-by-layer assemblies

* To whom correspondence should be addressed. Fax (847) 491 3010. E-mail: s-stupp@northwestern.edu.
[†] Department of Materials Science and Engineering, Northwestern University.
[‡] Department of Chemistry, Northwestern University.
[§] Feinberg School of Medicine, Northwestern University.

10.1021/jp077589+ CCC: $40.75
Published on Web 02/02/2008

rather than a one-step EISA process. The high solubility of our amphiphiles in polar solvents allows for EISA to occur with the electronically active OPV as the lone surfactant without the need for dilution with nonconjugated surfactants. The molecular architecture of our OPV surfactant differs from that of surfactants typically used in EISA systems because it includes the use of positively charged head groups at both termini of the molecule as opposed to the common surfactant with a charged head group at only one terminus. As such, its symmetric structure also differs from the asymmetric nature of the other previously reported conjugated surfactant systems.[34−36] Our initial studies on energy transfer of these self-assembling hybrids showed nanoscale ordering;[37] however, the resulting nanostructure was not fully characterized. In EISA systems, structural characterization by X-ray techniques is used to gain a better understanding of the process itself as well as to optimize conditions and tune the final mesostructure for specific applications. Grazing-incidence X-ray scattering (GIXS) is a powerful and nondestructive technique that is used to identify the in-plane, as well as out-of-plane, structure of thin films[42] and has therefore been used to characterize EISA-formed nanostructured films.[43−47] In this work we have characterized the nanoscale structure of the hybrid systems using GIXS as well as specular X-ray reflectivity (XRR) and powder X-ray diffraction (XRD). Two different systems were investigated in this study; one was the previously studied silica−OPV amphiphile hybrid and a second one containing silica and a novel amphiphile with a more conductive tetrameric oligo(thiophene) as the conjugated segment.

Experimental Methods

General. Unless otherwise noted, all starting materials were obtained from commercial suppliers and used without further purification. ^{1}H NMR and ^{13}C NMR spectra were recorded in a Varian Inova 500 (500 MHz for ^{1}H and 120 MHz for ^{13}C NMR) spectrometer using the solvent proton signal as standard. Mass spectra were obtained on a Micromass Quattro II atmospheric pressure ionization (API) triple quadrupole mass spectrometer. Matrix-assisted laser desorption ionization time-of-flight mass spectrometry (MALDI-TOF MS) was performed on an Applied Biosystems Voyager-DE Pro. XRD patterns were recorded using a Rigaku ATX-G X-ray diffractometer at an operating power of 50 kV and 240 mA with a Cu Kα (8.05 keV, 1.54 Å) source.

Synthesis. OPV amphiphiles were synthesized using the Horner−Wadsworth−Emmons reaction for the formation of *trans*-vinyl bonds and subsequent alkylation of the tertiary amines to the quaternary ammonium salts. Full details of the synthetic procedure are provided in ref 37. Thiophene amphiphiles were synthesized as described in the Supporting Information using a Stille reaction for the formation of the thiophene core and subsequent alkylation of the tertiary amine to form tetramethylammonium salts.

Film Preparation. Precursor solutions of the amphiphile/silica hybrid films were prepared by first dissolving 6.0 mg of the amphiphile in 1.0 mL of MeOH. Solutions were ultrasonicated to fully dissolve the amphiphile, and then 15 μL of 35 wt % aqueous HCl and 14 μL of tetraethyl orthosilicate (TEOS) were added for a molar ratio of 1:6.67 (**1**/TEOS) or 1:7.23 (**2**/TEOS). For concentration-dependent studies, the ratio of amphiphile to TEOS was varied by adjusting the amount of TEOS and acid added to the amphiphile solution. Hydrolysis and condensation of the TEOS to form silica and subsequent interaction with the charged end groups of the amphiphile occurred during solution stirring for 30 min at room temperature. Solutions of the pure OPV amphiphile films were prepared by dissolving 6.0 mg of the amphiphile in 1.0 mL of MeOH and further sonicating for full dissolution. All solutions were membrane filtered (pore size: 0.45 μm) and deposited on 2.5 cm × 2.5 cm float glass substrates by spin-casting at 1000 rpm for 30 s. Substrates were treated prior to deposition in piranha solution (7:3 (v/v) H_2SO_4/H_2O_2 (30% aq)) for 10 min at 100 °C to remove organic contaminants from the surface followed by rinsing with DI water, soaking in (4:1 (v/v) NH_4OH/H_2O_2 (30% aq)) for 5 min, rinsing with ultrapure 18 MΩ cm water and finally drying under a stream of dry nitrogen. *Caution: piranha solution is an extremely dangerous oxidizing agent and should be handled with care.* The films were left overnight at ambient atmosphere and subsequently dried under high vacuum for 3 h for full solvent evaporation.

GIXS. GIXS measurements were carried out at the 5ID-C beam line of the Advanced Photon Source (APS) at Argonne National Laboratory at an energy of 12.4 keV (1.00 Å wavelength). The incident angle was set at or near the critical angle for the glass substrate ($q_c = 0.032$ Å^{-1}) to enhance scattering from the film with a MAR CCD 2D area detector located 340 mm away from the sample for the OPV studies. The detector was located 388 mm away from the sample for measurements on the thiophene derivative. The sample was kept under flowing nitrogen so as to prevent ozone formation and minimize radiation damage. Frames were collected for 30−100 s.

Specular XRR. Measurements of the pure OPV amphiphile films and initial measurements of the hybrid films were made using a Rigaku ATX-G instrument at an operating power of 50 kV and 240 mA with a Cu Kα (8.04 keV, 1.54 Å) source and incident beam size of 0.1 mm. Further XRR of the hybrid films was performed at the 5ID-C beam line of the APS at an energy of 12.4 keV (1.00 Å wavelength). Collected reflectivity scans were background subtracted and normalized to the ideal Fresnel reflectivity for float glass.

Results and Discussion

GIXS Measurements. In our first structural characterization of the OPV/silica hybrid, specular XRR yielded first- and second-order Bragg peaks corresponding to *d* spacings of 2.76 and 1.37 nm.[37] We proposed that these two out-of-plane peaks could be assigned possibly to a lamellar structure. However, a hexagonal structure could be present in these systems resulting from the packing of cylindrical micelles aligned parallel to the substrate, and giving rise only to (01) and (02) reflections so that the (11) reflection would not be observed. To probe the ordering in these films along the in-plane and surface normal directions and determine their nanoscale structure, GIXS measurements were performed at the APS with a 2D area CCD detector. The GIXS patterns for the OPV/silica hybrids films are shown in parts a−c of Figure 1with momentum transfer reciprocal space coordinates q_x-q_z, where q_z is the out-of-plane direction, and q_x is in-plane and perpendicular to the incident beam.[48] All three patterns show a slightly distorted 2D hexagonal phase with the out-of-plane vector slightly shorter than the in-plane. To take into account this distortion, a rectangular face-centered unit cell with lattice parameters a_{rec} and c_{rec}, was used to index the diffraction spots and represent the vertically strained hexagonal lattice (see Figure 2).

Figure 1b shows the pattern generated by the film mineralized with a starting molar ratio of tetraethyl orthosilicate (TEOS) to OPV of 6.67, the same amount used in our previous work in ref 37 for the energy transfer experiments with rhodamine. When

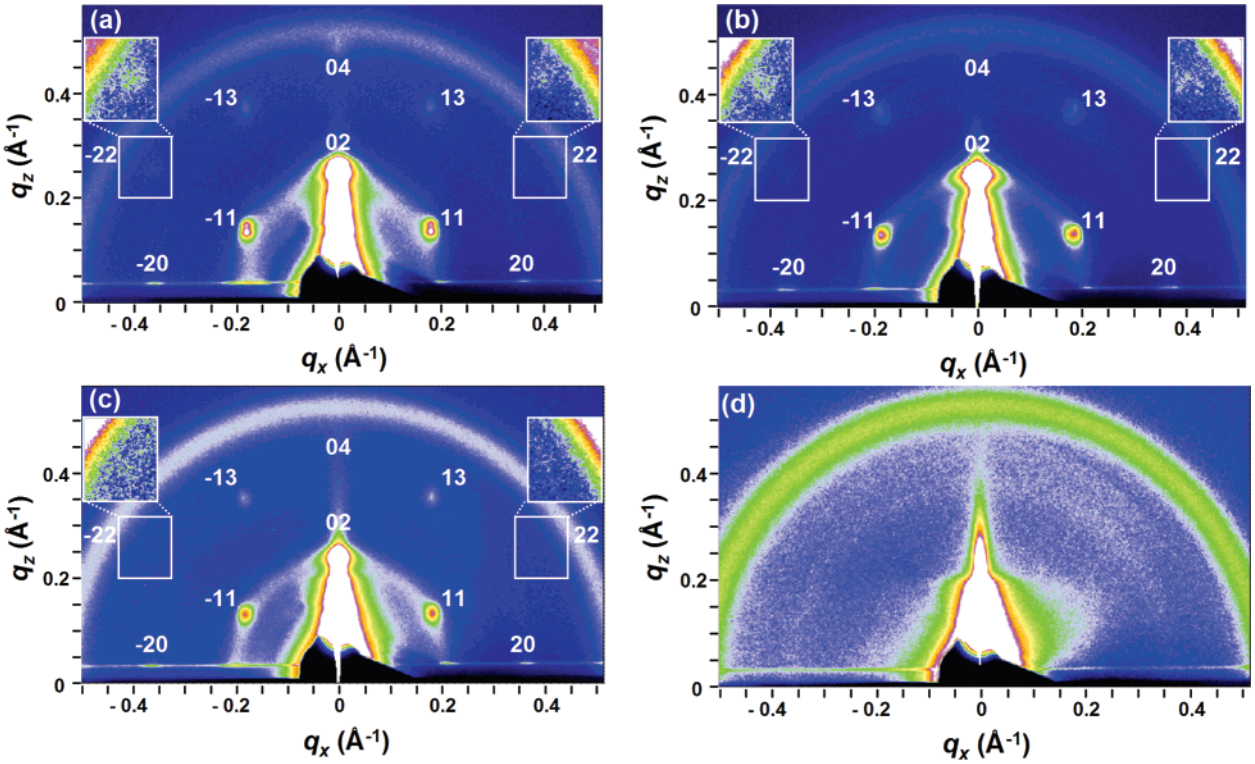

Figure 1. Grazing-incidence 2D X-ray scattering patterns identifying vertically strained hexagonal packing for OPV amphiphile (**1**)/silica films and lack of ordering in unmineralized OPV film. Listed *hl* indices for each Bragg peak are in reference to the 2D rectangular face-centered unit cell. The starting molar ratios of **1**/tetraethyl orthosilicate of: (a) 1:10, (b) 1:6.67, (c) 1:3.33, (d) 1:0. Insets show magnified portions of weaker intensity peaks.

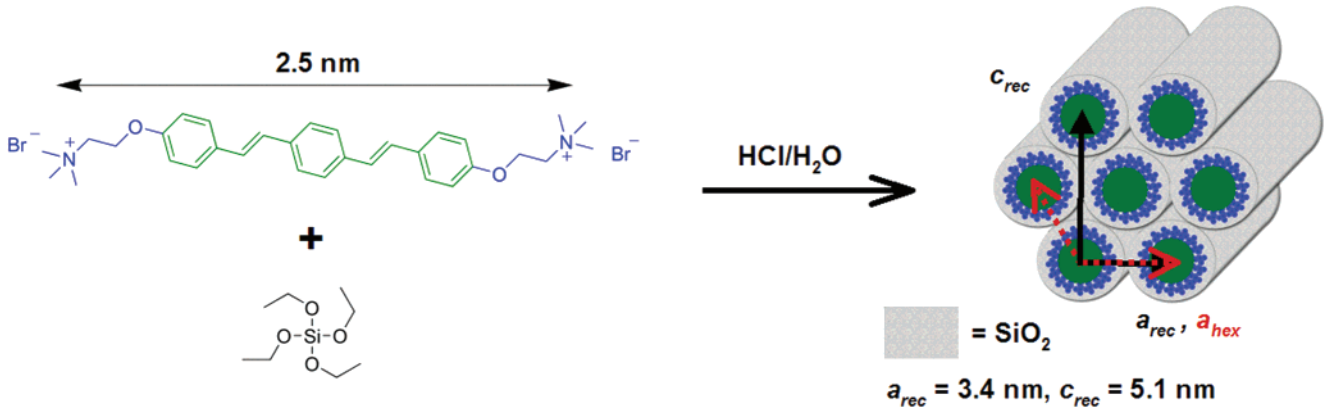

Figure 2. Schematic of evaporation-induced self-assembly process. Initial solution of OPV amphiphiles (**1**) and silica precursor, TEOS, forms vertically strained hexagonally packed cylindrical micelles with their axes lying parallel to the surface planar. The 2D hexagonal (hex) unit cell axes are shown as red-dashed line vectors. The 2D rectangular face-centered (rec) unit cell axes are indicated by black arrows with c_{rec} along the surface normal.

the observed diffraction spots are indexed, a_{rec} is found to be equal to 3.4 nm and c_{rec} = 5.1 nm. This characterizes the nanoscale structure as distorted cylinders with diameters of 3.4 nm parallel to the substrate and 3.1 nm out-of-plane. For an undistorted 2D hexagonal lattice, the ratio of the rectangular face-centered lattice spacings would be $c_{rec}/a_{rec} = \sqrt{3}$. The one-dimensional shrinkage of the cylinders normal to the substrate creates elliptical rather than perfectly circular shapes for the cylindrical cores. This effect has been previously attributed to vertical compressive strain caused by drying effects and siloxane condensation occurring after the hexagonal mesophase forms.[44−47,49] The hexagonally packed cylindrical micelles are formed in the hybrid films oriented parallel to the substrate surface. As observed in all previous work on hexagonal mesoporous silica, we expect the conjugated surfactants to orient transverse to the long axis of the pores (see Figure 2). The fully extended length of the OPV amphiphile (**1**) shown below is approximately 2.5 nm, and therefore the observed overall cylinder diameters, 3.4 nm in-plane and 3.1 nm out-of-plane, are consistent with transverse orientation of the molecules with silica shells formed around them. The charged end groups of the amphiphiles are expected to interact with TEOS, the silica precursor, and thus the inorganic material should coat the exterior of the cylindrical aggregates of conjugated molecules.

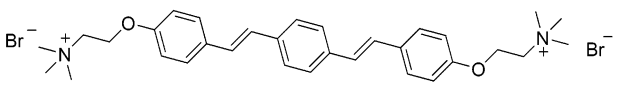

1

To test the generality of this self-assembling hybrid system with a different amphiphile, we used a more conductive

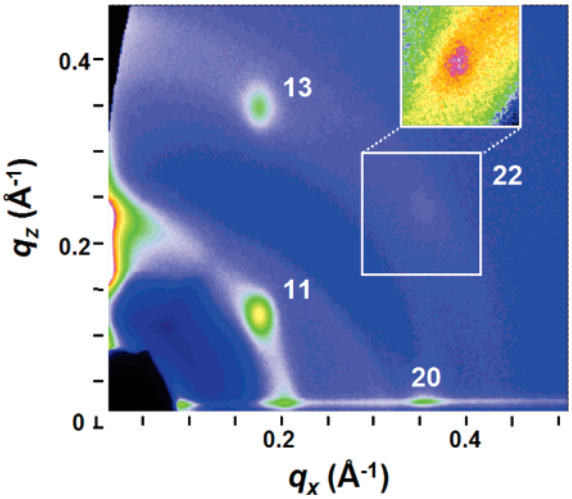

Figure 3. Grazing-incidence 2D X-ray scattering patterns identifying vertically strained hexagonal packing for oligo(thiophene) amphiphile (**2**)/silica film for one quadrant of q_x-q_z. Listed *hl* indices for each Bragg peak are in reference to the 2D rectangular face-centered unit cell. Inset shows magnified portion of weaker intensity peak.

conjugated segment. We successfully synthesized the quaterthiophene analogue (**2**) of the surfactant shown below. Interestingly, upon mineralization with silica we obtained the same distorted hexagonally packed cylindrical micelle nanostructured films. Figure 3 shows the CCD image obtained for one quadrant of the q_x-q_z plane for a film prepared from a 1-mL solution in MeOH of 6 mg of **2** and 14 μL of TEOS with a molar ratio of TEOS to **2** of 7.23, close to the ratio of the original OPV hybrid of 1:6.67 (**1**/TEOS). In the case of **2**, the slightly longer extended molecular length of 2.8 nm compared to **1** (2.5 nm) is also reflected in a slight increase of the unit cell dimensions with a_{rec} = 3.6 nm and c_{rec} = 5.8 nm. This leads to cylinder dimensions of 3.6 nm parallel to the substrate and 3.4 nm out-of-plane. This result using GIXS on a second compound supports our expectation that the conjugated molecules are oriented perpendicular to the long axis of a one-dimensional cylindrical aggregate and surrounded by silica.

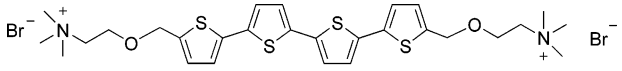

2

In comparison to a surfactant molecule such as cetyltrimethylammonium bromide (CTAB), not only are hydrophobic interactions important in our case, but $\pi-\pi$ stacking interactions among the conjugated amphiphiles should also promote aggregation of the OPV or thiophene segments. We assume that twisting of the amphiphiles within the π-stacked aggregates along the long axis gives rise to the uniaxial symmetry observed. We also believe that the symmetric dual charge nature of our amphiphiles and the subsequent interactions with silica precursors might give rise to long-range ordering in our nanostructured hybrid films.

The observed diffraction spots do not change their positions when samples are rotated about their surface normal direction. This indicates the presence of individual domains consisting of aligned hexagonally packed cylinders. The cylindrical axis of each domain is aligned parallel to the surface, but there is no preferred in-plane orientation for these domains. While most of the domains lie flat on the substrate, the faint powder rings produced around the diffraction spots indicate that a small fraction of the domains are randomly oriented.

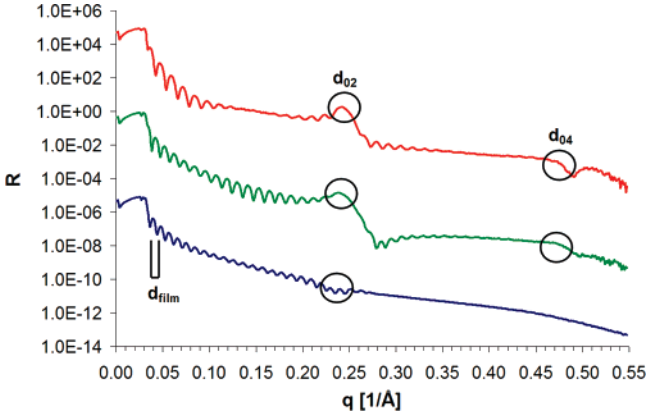

Figure 4. Specular X-ray reflectivity data for mineralized OPV films with starting molar ratios of **1**/tetraethyl orthosilicate of 1:3.33 (red), 1:6.67 (green), and 1:10 (blue).

In order to study the effect of the molar ratio of silica on the final overall structure, two more hybrid film samples were prepared by maintaining a constant concentration of **1** (6 mg/mL) and either increasing or decreasing the molar concentration of TEOS and proportionally the acid catalyst, HCl, in order to minimize siloxane condensation and ensure cooperative assembly of the surfactant and silica.[28] In these cases, the same pseudo-hexagonal packing or rectangular face-centered unit cell is generated. In fact, the resulting *d* spacings and cylinder dimensions remain constant for the unit cell in all three cases with starting molar ratios of TEOS to **1** of (a) 10, (b) 6.67, and (c) 3.33 equiv. Because the cylinder dimensions do not change with the amount of TEOS, the results suggest that there is a maximum molar ratio of TEOS that will interact with the fixed number of charged end groups of OPV amphiphilic molecules to generate the hexagonally packed nanoscale structure. When more TEOS is added, this fixed number of charged end groups on **1** prevents further silica from being incorporated around the cylindrical aggregates. Our XRR studies suggest that the additional silica formed is not incorporated within the cylindrical hybrid nanostructure (vide infra). As we previously reported, a uniform distribution of the amphiphiles is implied by the linear relationship between the optical density and film thickness of the hybrids.[37] In the absence of TEOS and the acid catalyst, a film cast from **1** in solution at the same concentration near its solubility limit of 9.0 mM did not lead to the hexagonal structure (see Figure 1d). This implies that the ordering observed is a direct result of the mineralization process.

Specular XRR Measurements. Specular XRR[50,51] was used to probe the periodicity along the surface normal q_z in order to obtain more information about the internal structure of the OPV hybrid films. This is possible since XRR is sensitive to planes parallel to the surface. For the sample with the lowest starting molar ratio of TEOS to **1** of 3.33, the specular reflectivity in Figure 4 yielded the first- and second-order allowed Bragg peaks corresponding to 2.6 and 1.3 nm, respectively. The peaks were also observed in the CCD image in Figure 1c and are assigned to the (02) and (04) diffractions of the rectangular face-centered unit cell. The overall film thickness is determined to be $2\pi/\Delta q_z$ = 48 nm, where Δq_z is the periodicity between the Kiessig fringes observed above the critical angle of the glass substrate (q_c = 0.032 Å^{-1}). These fringes result from the interference between the different interfaces reflected along the surface normal direction.[52]

The Patterson function, $P(z)$ (Fourier transform of the reflectivity normalized by the Fresnel reflectivity for an ideally flat glass mirror), is shown in Figure 5a. The observed peaks

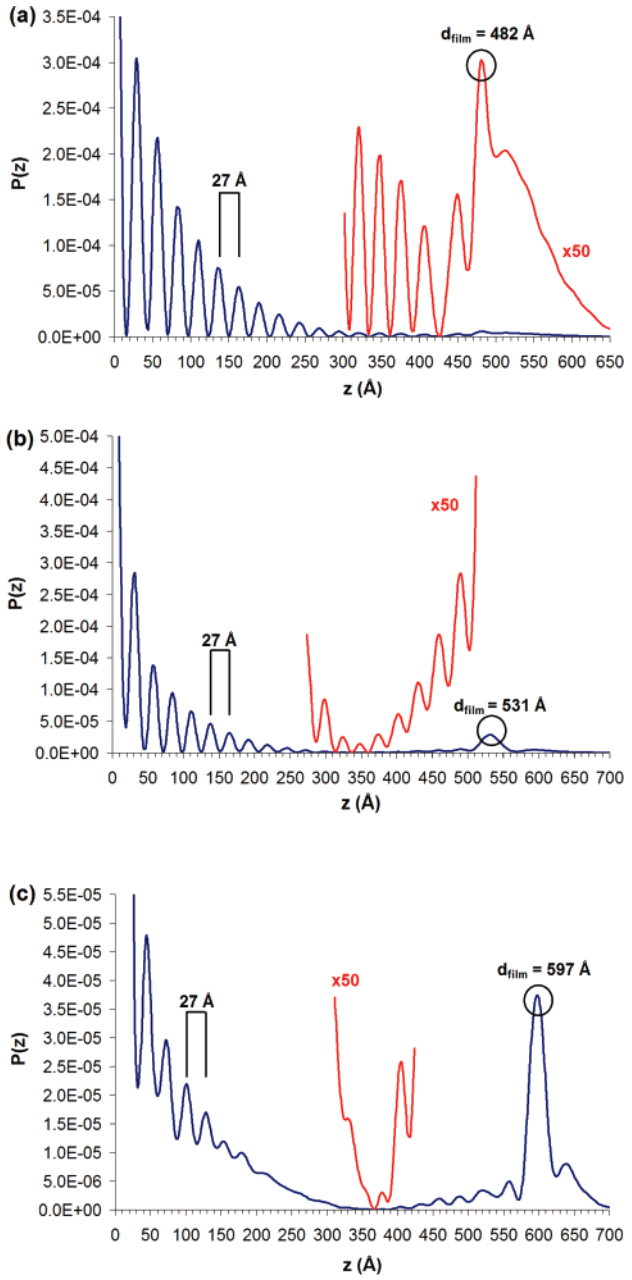

Figure 5. Patterson map of mineralized OPV films with starting molar ratios of **1**/tetraethyl orthosilicate of (a) 1:3.33, (b) 1:6.67, and (c) 1:10 with red insets showing magnified views.

correspond to the distances between any two interfaces which are sensed by a change in electron density.[50,51] The distance between these peaks had an average value of 2.7 nm that closely matches the position of the first-allowed Bragg peak. These peaks are evident along the entire film profile, indicating that the periodicity of the hexagonally packed cylinders exists throughout the q_z direction. The peak at 48 nm corresponds to the overall film thickness. Profilometry on all films matched the thicknesses obtained from XRR measurements.

When the initial molar ratio of TEOS to **1** is 6.67, the specular reflectivity again generates the first- and second-order allowed Bragg peaks corresponding to the (02) and (04) peaks of the rectangular face-centered unit cell (see Figure 4). The well-pronounced oscillations throughout the angular range indicate a homogeneous and uniform film. While the nanoscale structure is maintained, it is clear that an increased amount of silica leads to an increase in the overall film thickness (53 nm) that is also evident in the Patterson function shown in Figure 5b. The Patterson map further indicates that the periodicity of the nanostructure exists along the entire film thickness profile.

The hybrid sample measured with the largest starting molar ratio of TEOS, 1:10 **1**/TEOS, also formed hexagonally packed cylindrical micelles in Figure 1a. However, the first-order allowed Bragg peak is no longer obvious, and the second-order peak completely disappears in the specular reflectivity in Figure 4. The interference fringes, which correspond to the film thickness (60 nm), disappear past the first-order allowed Bragg peak. This damping of the thickness fringes and their appearance within a narrower angular range implies that the roughness of the film is higher than for other samples. Further inspection of the Patterson map in Figure 5c shows a dampening of the periodicity peaks within the middle of the film thickness profile, indicating that while the film is highly ordered at both its bottom and top, disorder does seem to exist in the middle of the film. This implies that with an increase in the starting amount of TEOS in relation to OPV conjugated amphiphiles the distorted hexagonal structure is still formed, but the additional silica formed is not incorporated within the periodic framework and instead exists as bulk silica in regions within the center of the film.

The control film cast from **1** in the absence of the silica precursor, which lacked any diffraction pattern in GIXS, also lacked any Bragg peaks in its specular reflectivity (see Figure 6). Well-ordered Kiessig fringes appear, indicating a smooth and uniformly homogeneous film, with a periodicity that matches the peak corresponding to the overall film thickness (37 nm) in the Patterson map. It is also clear from the Patterson map that, without the addition of TEOS, **1** does not form a highly ordered structure. Only a few peaks exist with a roughly 2.2 nm distance separating them that might correspond to the length of the molecule between the two oxygen atoms. However, this ordering is not very pronounced and does not occur throughout the entire film. While some rather weak ordering might exist, we believe that, due to the bolaform of the amphiphile, the absence of silica prevents the charge-shielding necessary to allow for any long-range packing of molecules with like charges at both termini. We further investigated by studying a molecule lacking the charges at opposite termini.

Role of Charge on Molecular Packing. The uncharged precursor to the OPV amphiphile (**3**) shown below contains dimethylamine groups on both termini and was used to investigate the role of charge on molecular packing. Attempts to cast a film of **3** from solution were unsuccessful due to its insolubility in organic solvents at sufficient concentrations. Consequently, measurements were made on the neat powder of the molecule and compared to the neat form of the cationic version used in mineralization to generate hybrid material. The X-ray powder diffraction pattern (Figure 7) of **3** indicates formation of a layered structure with *d* spacings of 2.71, 1.36, and 0.91 nm corresponding to (001), (002), and (003) reflections, respectively. The first-order peak is slightly larger than the fully extended length of the molecule between the two nitrogens (2.5 nm), suggesting a layered packing of the molecule. With the addition of charges to the end groups, however, the cationic OPV **1** only generates an extremely faint peak, almost 2 orders of magnitude weaker in intensity than the first-order peak of the uncharged analog at 2.1 nm. This peak corresponds roughly to the distance between the alkyl chains on either end. This observation strongly suggests that repulsion between like charges disrupts long-range ordering of the molecules. The widths of the peaks in the bis-tertiary amine indicate that domains of

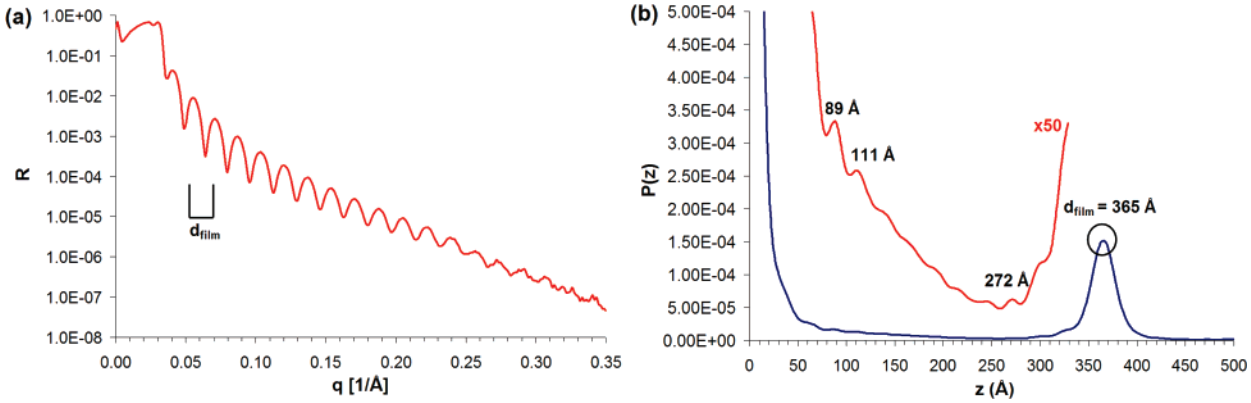

Figure 6. Specular X-ray reflectivity of unmineralized OPV (**1**) film (a) and resulting Patterson map with red curve showing a magnified view (b).

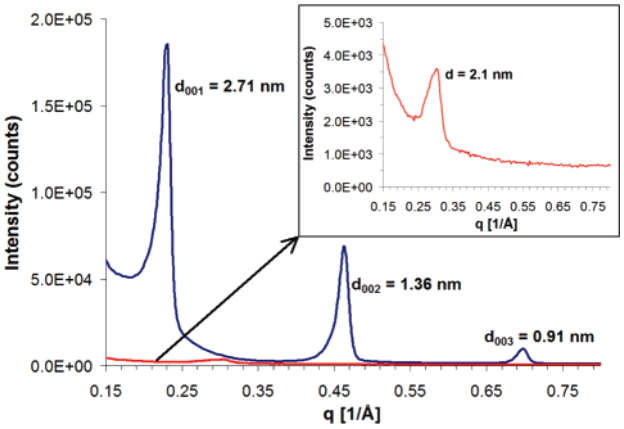

Figure 7. X-ray powder diffraction of neat OPV amphiphile (**1**) used for mineralization with charged termini and bromine ions (red line) and of the neat uncharged precursor (**3**) (blue line). Inset shows magnified view of spectrum for **1**.

uncharged molecules are larger than those of the cationic amphiphile. The results suggest that the single lone broad peak for the cationic amphiphile is due to weak ordering from small domains. We believe that this weak ordering is due to the small fraction of rigid cores that are able to π-stack in the presence of the charged groups at the termini of molecules. We conclude that the highly charged nature of the conjugated amphiphiles is very important to the development of long-range order in the self-assembling hybrid materials investigated. In the absence of mineralization, charges on these molecules clearly disrupt packing, but binding of TEOS by the end groups and the subsequent mineralization screens charges in the cationic amphiphiles. This screening, in turn, allows the possibility of forming the long range order observed in the hexagonal phase of the hybrid. On the basis of curvature-packing arguments,[53] as well as the similar behavior of CTAB that has been previously reported,[44] we conclude that the aggregates of conjugated molecules are sterically forced into the curved hexagonal structure as the film is formed and solvent is evaporated. This results in the transformation from a lamellar to a hexagonal nanostructure. The presence of two binding sites for TEOS per molecule and their ability to π-stack may also be a contributing force to the transformation and the long-range order observed in these hybrid structures.

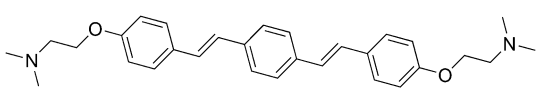

3

Conclusions

Conjugated amphiphiles containing two charged groups and silica precursors can spontaneously form hybrid structures with long-range order and hexagonal symmetry. Silica coats the exterior of the hexagonally packed cylindrical micelles composed of aggregated conjugated molecules. Experiments with uncharged organic analogues suggest that screening of the doubly charged amphiphiles by the mineralization process leads to long-range order in these hybrid materials. Long-range order and the electronic function in the organic compartments of these hybrid structures suggest their use in self-assembling photovoltaic systems with proper choice of a conductive composition in the inorganic phase.

Acknowledgment. This work was supported by the U.S. Department of Energy under Award DE-FG02-00ER54810. The work made use of the Jerome B. Cohen X-ray Diffraction Facility and the Analytical Services Laboratory at Northwestern University. We acknowledge facilities support by the Materials Research Center through NSF MRSEC Grant DMR-0520513. This work was partially supported by the Nanoscale Science and Engineering Center through NSF Grant EEC-0118025. GIXS and XRR measurements were performed at the DuPont−Northwestern−Dow Collaborative Access Team (DND-CAT) Synchrotron Research Center located at Sector 5 of the Advanced Photon Source. DND-CAT is supported by the E.I. DuPont de Nemours & Co., The Dow Chemical Company, the U.S. National Science Foundation through Grant DMR-9304725, and the State of Illinois through the Department of Commerce and the Board of Higher Education Grant IBHE HECA NWU 96. Use of the APS was supported by the U.S. Department of Energy, Office of Science, Office of Basic Energy Sciences, under Contract No. W-31-109-Eng-38. The authors thank Liangshi Li and Keisuke Tajima for useful discussions and Leiming Li for assistance with initial X-ray measurements. The authors also thank the DND-CAT staff, particularly Denis T. Keane for providing assistance with the experimental setup and technical support.

Supporting Information Available: Full synthetic procedure and scheme of quaterthiophene amphiphile. This material is available free of charge via the Internet at http://pubs.acs.org.

References and Notes

(1) Sanchez, C.; Soler-Illia, G.; Ribot, F.; Lalot, T.; Mayer, C. R.; Cabuil, V. *Chem. Mater.* **2001**, *13*, 3061−3083.

(2) Gomez-Romero, P. *Adv. Mater.* **2001**, *13*, 163−174.

(3) Sanchez, C.; Lebeau, B.; Chaput, F.; Boilot, J. P. *Adv. Mater.* **2003**, *15*, 1969−1994.
(4) Caseri, W. *Macromol. Rapid Commun.* **2000**, *21*, 705−722.
(5) Colvin, V. L.; Schlamp, M. C.; Alivisatos, A. P. *Nature* **1994**, *370*, 354−357.
(6) Konenkamp, R.; Word, R. C.; Godinez, M. *Nano Lett.* **2005**, *5*, 2005−2008.
(7) Lee, T. W.; Park, O. O.; Yoon, J. H.; Kim, J. J. *Adv. Mater.* **2001**, *13*, 211−213.
(8) O'Regan, B.; Gratzel, M. *Nature* **1991**, *353*, 737−740.
(9) Huynh, W. U.; Dittmer, J. J.; Alivisatos, A. P. *Science* **2002**, *295*, 2425−2427.
(10) Coakley, K. M.; McGehee, M. D. *Appl. Phys. Lett.* **2003**, *83*, 3380−3382.
(11) Beek, W. J. E.; Wienk, M. M.; Kemerink, M.; Yang, X. N.; Janssen, R. A. J. *J. Phys. Chem. B* **2005**, *109*, 9505−9516.
(12) Mann, S.; Ozin, G. A. *Nature* **1996**, *382*, 313−318.
(13) Stupp, S. I.; Braun, P. V. *Science* **1997**, *277*, 1242−1248.
(14) Estroff, L. A.; Hamilton, A. D. *Chem. Mater.* **2001**, *13*, 3227−3235.
(15) Mann, S.; Burkett, S. L.; Davis, S. A.; Fowler, C. E.; Mendelson, N. H.; Sims, S. D.; Walsh, D.; Whilton, N. T. *Chem. Mater.* **1997**, *9*, 2300−2310.
(16) Weiner, S.; Addadi, L. *J. Mater. Chem.* **1997**, *7*, 689−702.
(17) Mann, S. *Nature* **1993**, *365*, 499−505.
(18) Braun, P. V.; Osenar, P.; Stupp, S. I. *Nature* **1996**, *380*, 325−328.
(19) Braun, P. V.; Osenar, P.; Tohver, V.; Kennedy, S. B.; Stupp, S. I. *J. Am. Chem. Soc.* **1999**, *121*, 7302−7309.
(20) Kresge, C. T.; Leonowicz, M. E.; Roth, W. J.; Vartuli, J. C.; Beck, J. S. *Nature* **1992**, *359*, 710−712.
(21) Beck, J. S.; Vartuli, J. C.; Roth, W. J.; Leonowicz, M. E.; Kresge, C. T.; Schmitt, K. D.; Chu, C. T. W.; Olson, D. H.; Sheppard, E. W.; McCullen, S. B.; Higgins, J. B.; Schlenker, J. L. *J. Am. Chem. Soc.* **1992**, *114*, 10834−10843.
(22) Huo, Q. S.; Margolese, D. I.; Ciesla, U.; Feng, P. Y.; Gier, T. E.; Sieger, P.; Leon, R.; Petroff, P. M.; Schuth, F.; Stucky, G. D. *Nature* **1994**, *368*, 317−321.
(23) Zhao, D. Y.; Feng, J. L.; Huo, Q. S.; Melosh, N.; Fredrickson, G. H.; Chmelka, B. F.; Stucky, G. D. *Science* **1998**, *279*, 548−552.
(24) Ogawa, M. *Chem. Commun.* **1996**, 1149−1150.
(25) Yang, H.; Kuperman, A.; Coombs, N.; MamicheAfara, S.; Ozin, G. A. *Nature* **1996**, *379*, 703−705.
(26) Yang, H.; Coombs, N.; Sokolov, I.; Ozin, G. A. *Nature* **1996**, *381*, 589−592.
(27) Nicole, L.; Boissiere, C.; Grosso, D.; Quach, A.; Sanchez, C. *J. Mater. Chem.* **2005**, *15*, 3598−3627.
(28) Brinker, C. J.; Lu, Y. F.; Sellinger, A.; Fan, H. Y. *Adv. Mater.* **1999**, *11*, 579−585.
(29) Fan, H. Y.; Brinker, J. *Stud. Surf. Sci. Catal.* **2004**, *148*, 213−240.
(30) Lu, Y. F.; Ganguli, R.; Drewien, C. A.; Anderson, M. T.; Brinker, C. J.; Gong, W. L.; Guo, Y. X.; Soyez, H.; Dunn, B.; Huang, M. H.; Zink, J. I. *Nature* **1997**, *389*, 364−368.
(31) Aida, T.; Tajima, K. *Angew. Chem., Int. Ed. Engl.* **2001**, *40*, 3803−3806.
(32) Ikegame, M.; Tajima, K.; Aida, T. *Angew. Chem., Int. Ed. Engl.* **2003**, *42*, 2154−2157.
(33) Lu, Y. F.; Yang, Y.; Sellinger, A.; Lu, M. C.; Huang, J. M.; Fan, H. Y.; Haddad, R.; Lopez, G.; Burns, A. R.; Sasaki, D. Y.; Shelnutt, J.; Brinker, C. J. *Nature* **2001**, *410*, 913−917.
(34) Bhongale, C. J.; Hsu, C. S. *Angew. Chem., Int. Ed. Engl.* **2006**, *45*, 1404−1408.
(35) Tsai, F. Y.; Tu, H. L.; Mou, C. Y. *J. Mater. Chem.* **2006**, *16*, 348−350.
(36) Clark, A. P. Z.; Shen, K. F.; Rubin, Y. F.; Tolbert, S. H. *Nano Lett.* **2005**, *5*, 1647−1652.
(37) Tajima, K.; Li, L.-S.; Stupp, S. I. *J. Am. Chem. Soc.* **2006**, *128*, 5488−5495.
(38) Sun, J. Z.; Sun, J. Q.; Ma, Y. G.; Zhang, X.; Shen, J. C. *Mater. Sci. Eng. C* **1999**, *10*, 83−86.
(39) Locklin, J.; Youk, J. H.; Xia, C. J.; Park, M. K.; Fan, X. W.; Advincula, R. C. *Langmuir* **2002**, *18*, 877−883.
(40) Xia, C.; Locklin, J.; Youk, J. H.; Fulghum, T.; Advincula, R. C. *Langmuir* **2002**, *18*, 955−957.
(41) Fan, X. W.; Locklin, J.; Youk, J. H.; Blanton, W.; Xia, C. J.; Advincula, R. *Chem. Mater.* **2002**, *14*, 2184−2191.
(42) Hillhouse, H. W.; van Egmond, J. W.; Tsapatsis, M.; Hanson, J. C.; Larese, J. Z. *Microporous Mesoporous Mater.* **2001**, *44*, 639−643.
(43) Grosso, D.; Cagnol, F.; Soler-Illia, G.; Crepaldi, E. L.; Amenitsch, H.; Brunet-Bruneau, A.; Bourgeois, A.; Sanchez, C. *Adv. Funct. Mater.* **2004**, *14*, 309−322.
(44) Doshi, D. A.; Gibaud, A.; Goletto, V.; Lu, M. C.; Gerung, H.; Ocko, B.; Han, S. M.; Brinker, C. J. *J. Am. Chem. Soc.* **2003**, *125*, 11646−11655.
(45) Grosso, D.; Babonneau, F.; Albouy, P. A.; Amenitsch, H.; Balkenende, A. R.; Brunet-Bruneau, A.; Rivory, J. *Chem. Mater.* **2002**, *14*, 931−939.
(46) Doshi, D. A.; Gibaud, A.; Liu, N. G.; Sturmayr, D.; Malanoski, A. P.; Dunphy, D. R.; Chen, H. J.; Narayanan, S.; MacPhee, A.; Wang, J.; Reed, S. T.; Hurd, A. J.; van Swol, F.; Brinker, C. J. *J. Phys. Chem. B* **2003**, *107*, 7683−7688.
(47) Gibaud, A.; Grosso, D.; Smarsly, B.; Baptiste, A.; Bardeau, J. F.; Babonneau, F.; Doshi, D. A.; Chen, Z.; Brinker, C. J.; Sanchez, C. *J. Phys. Chem. B* **2003**, *107*, 6114−6118.
(48) Due to the Kapton foil placed over the sample with flowing N_2 to prevent ozone formation and minimize radiation damage, a Kapton powder diffraction ring intersecting d_{04} is evident in Figure 1b, and throughout all the GIXS CCD images. An oversaturation along the q_z axis is observed due to the strong intensity along the specular direction.
(49) Gibaud, A.; Baptiste, A.; Doshi, D. A.; Brinker, C. J.; Yang, L.; Ocko, B. *Europhys. Lett.* **2003**, *63*, 833−839.
(50) Daillant, J.; Gibaud, A. *X-Ray and Neutron Reflectivity: Principles and Applications*; Springer: Berlin, 1999.
(51) Tolan, M. *X-Ray Scattering from Soft-Matter Thin Films: Materials Science and Basic Research*; Springer: Berlin, 1999; Vol. 148.
(52) Kiessig, H. *Ann. Phys.* **1931**, *10*, 769.
(53) Israelachvili, J. *Intermolecular and Surface Forces*; Elsevier Science: London, 2002.